# Crystalline Microporous MoVBiO Polyoxometalates for Indirect Oxidation of Methanol to Methyl Formate: Effects of Organic Additives on Crystals Size and Catalytic Performance

Ke Huang, Ningkun Xu, Bin Liu, Peihua Zhang, Ge Yang, Hailing Guo, Peng Bai, Chunzheng Wang, Svetlana Mintova

# Crystalline Microporous MoVBiO Polyoxometalates for Indirect Oxidation of Methanol to Methyl Formate: Effects of Organic Additives on Crystals Size and Catalytic Performance

Ke Huang,[a] Ningkun Xu,[a] Bin Liu,[a] Peihua Zhang,[a] Ge Yang,[a] Hailing Guo,[a] Peng Bai,[a] Chunzheng Wang,*[,a] and Svetlana Mintova*[,a],[b]

[a] *State Key Laboratory of Heavy Oil Processing, College of Chemistry and Chemical Engineering, China University of Petroleum (East China), Qingdao 266580, Shandong, China*

[b] *Laboratoire Catalyse et Spectrochimie (LCS), Normandie Université, ENSICAEN, UNICAEN, CNRS, 6 boulevard Maréchal Juin, Caen 14050, France*

* Corresponding authors. E-mail addresses: czwang@upc.edu.cn (C. Wang), svetlana.mintova@ensicaen.fr (S. Mintova)

## Abstract

Crystalline porous Mo-V-Bi oxides (MoVBiO) were prepared by hydrothermal synthesis approach. The effects of organic additives (methanol and tartaric acid) on the morphology and particle size of the MoVBiO crystals were investigated. The size of MoVBiO crystals was tuned in the range of 30–300 nm. It was found that the methanol accelerated the formation of crystal nuclei resulting in the crystallization of small particles (30 nm), while the tartaric acid inhibited the nucleation thus resulting in MoVBiO crystals with a size of 300 nm. The as-synthesized MoVBiO samples

were used in the indirect oxidation of methanol to methyl formate. The MoVBiO crystals with a size of 30 nm synthesized with methanol, showed a high methyl nitrite conversion of 92 % and methyl formate selectivity of 94 % at 140 °C. The catalyst exhibited a relatively slow but almost constant deactivation over 50 h due to the deposit of reaction species. The small MoVBiO crystals (30 nm) with more surface active sites and accessibility showed high performance in the oxidation of methanol to methyl formate in contrast to the big crystals (300 nm).

**Keywords:** Polyoxometalate; MoVBiO; Size effect; Methanol; Methyl formate

## Introduction

Polyoxometalates (POMs) are anionic metal oxide clusters comprised of transition metals such as molybdenum, vanadium, and tungsten.[1–3] POMs-based materials have well-defined building units forming ordered crystalline oxides, such as polyoxometalate-organic frameworks,[4–6] macrocations-POMs,[7–10] and multiple metal frameworks.[11–14] The properties of POMs, such as acidity, redox, magnetic and porosity, are highly tunable through changing their structures and incorporation of various metal components into the frameworks.[15] Therefore, POMs have been considered for various applications, such as catalysis,[16–19] adsorption,[20,21] separation[8,22] and others[3,23]. One example is the $(NH_4)_{2.8}H_{0.9}[\varepsilon\text{-}VMo_{9.4}V_{2.6}O_{40}–Bi_2]\cdot 7.2H_2O$, formed by connecting ε-Keggin POMs units, $(VMo_{9.4}V_{2.6}O_{40})^{-9.7}$ with $Bi^{3+}$ ions as a linker.[24] One $VO_4$ tetrahedron is

surrounded by twelve $MoO_6$ or $VO_6$ octahedrons generating the ε-Keggin POMs unit. Other example is the POMs containing Mo, V and Bi (MoVBiO) with a diamond-like framework containing cages and channels; the crystal structure and the pore system of the MoVBiO resemble the FAU-type zeolite.[25] The MoVBiO framework structure contains three types of metal sites including central, surrounding and linked ones. These metal sites play different roles in catalytic reactions through facilitating the conversion of reactants and intermediates, and the desorption of products.[26,27] Ishikawa et al. reported on the use of MoVBiO in comparison to the crystalline $Mo_3VO_x$ in the ammoxidation of propane.[28] The propane conversion and acrylonitrile selectivity were improved using the MoVBiO catalyst. However, the pores of MoVBiO (seven-membered ring with a size of 0.34 nm), are too small for common molecules such as $N_2$, $CH_4$ and $CH_3OH$ to enter into the channels.[29] Hence, it is important to consider tuning of the particle size of the MoVBiO crystals in order to provide accessible active sites on the external surface and thus to enhance their performance in catalysis (activity/selectivity).

Methyl formate (MF) is an important organic synthesis intermediate in C1 chemistry, and has been widely used for the production of more than 50 chemicals, such as formic acid, formamide, dimethyl carbonate, ethylene glycol, and N,N-dimethylformamide.[30] MF is also applied as a precursor in the manufacture of pharmaceuticals and as a fuel additive.[31] The most common commercial route to synthesize MF is the liquid-phase methanol carbonylation which was industrialized by BASF in 1925.[32] The used sodium methoxide catalyst exhibited a high selectivity of

MF, but was sensitive to the moisture and caused the corrosion of equipment due to its high alkalinity.[33] The dehydrogenation of methanol to MF was classically performed in a fixed-bed reactor with copper-based catalysts. This process was only used in the small-scale industrial production due to the thermodynamic equilibrium and polymerization of formaldehyde on the catalyst surface.[34,35] The partial oxidation of methanol to MF as a strong exothermic reaction was thermodynamically more favorable than the dehydrogenation, but still is the focus of intense research.[36] The hydrocondensation of $CO_2$ with methanol is a green route to produce MF because it transferred the $CO_2$ emission gas to high-value products. Since $CO_2$ is a thermodynamic stable molecule, a high activation energy and great quantities of $CO_2$ at high pressure were necessary to proceed the reaction.[37,38] In addition, the photocatalytic oxidation of methanol is an innovative and sustainable approach for MF synthesis.[39] The photocatalytic reaction required targeted irradiation, and thus an industrial scale implementation seemed not foreseeable.[40] Hence, there is still a great need to develop highly efficient and environmental sustainable process for MF production.

Zhuo et al. proposed an indirect oxidation of methanol to MF via the methyl nitrite ($CH_3ONO$).[30] This indirect route for MF synthesis involves two separate reactions (Scheme S1 in Supporting Information (SI)): (1) non-catalytic synthesis of methyl nitrite ($CH_3ONO$) with $CH_3OH$ and $O_2$: $2CH_3OH + 2NO + 1/2O_2 \rightarrow 2CH_3ONO + H_2O$ and (2) MF synthesis: $4CH_3ONO \rightarrow CHOOCH_3 + 2CH_3OH + 4NO$ (the formed NO and methanol could be recycled for the synthesis of $CH_3ONO$).

The overall reaction ($2CH_3OH + O_2 \rightarrow CHOOCH_3 + 2H_2O$) results in an environmentally benign and highly efficient process. Zhuo et al. found that the zeolite catalyst (H-Y) exhibited a $CH_3ONO$ conversion of 83% and MF selectivity of 90% at 140 °C, and suggested that the acidic sites of the catalysts played a crucial role for the catalytic activity.[30] However, little attention was paid to the indirect route for MF synthesis, possibly due to the difficulty of $CH_3ONO$ regeneration. In 2010, the gas-phase carbonylation of $CH_3ONO$ to dimethyl oxalate has been industrially implemented, which is a crucial step from syngas to ethylene glycol via the dimethyl oxalate hydrogenation.[41] The carbonylation of $CH_3ONO$ to dimethyl oxalate consisted of two reactions: (1) $2CH_3ONO + 2CO \rightarrow 2NO + (CH_3OCO)_2$ and (2) $2NO + 2CH_3OH + 1/2O_2 \rightarrow 2CH_3ONO + H_2O$. The indirect route for MF is similar to the synthesis of dimethyl oxalate via the $CH_3ONO$ agent at moderate conditions. Designing high-performance catalysts for the indirect route to MF is desirable for both fundamental research and commercial application.

Herein, we presented a method to tune the size of MoVBiO using organic additives. The effects of the organic additives (methanol and tartaric acid) on crystal size of MoVBiO were investigated along the hydrothermal synthesis. The as-synthesized MoVBiO material was tested in the indirect oxidation of methanol to MF. The effect of crystal size of the MoVBiO on the catalytic performance in the MF synthesis was disclosed.

## Results and discussion

### Synthesis of MoVBiO samples with different sizes

Samples MoVBiO-M-120, MoVBiO-T-120 and MoVBiO-T-175 were synthesized with methanol and tartaric acid additives, respectively, while the MoVBiO-N-120 was prepared in the absence of organic additive. The XRD patterns of the samples are presented in Figure 1. The Bragg peaks at 2 Theta of 7.7, 19.6, 23.3, 25.4, 26.6 and 29.9 ° indexed as (111), (331), (511), (440), (531) and (622) reflections are detected, and consistent with the previously synthesized MoVBiO crystals.[15]

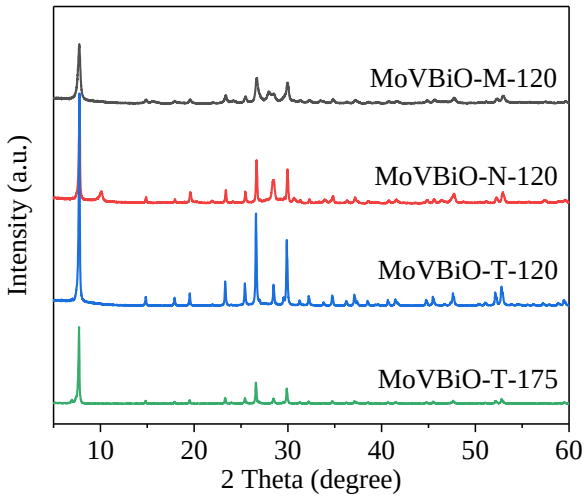


**Figure 1.** XRD patterns of samples MoVBiO-M-120, MoVBiO-N-120, MoVBiO-T-120 and MoVBiO-T-175.

The FTIR spectra of samples MoVBiO-M-120, MoVBiO-N-120, MoVBiO-T-120 and MoVBiO-T-175 are shown in Figure 2. The spectra are coherent with the ε-Keggin POM-based transition metal oxides reported earlier.[15,42] The band at 1637 $cm^{-1}$ is assigned to water, and the band at 1400 $cm^{-1}$ to $NH_4^+$.[25] The two

bands below 1000 $cm^{-1}$ are originated from the ε-Keggin POM unit.[42] The band at 981 $cm^{-1}$ is ascribed to Mo=O terminal bond, and the band at 811 $cm^{-1}$ corresponds to the Mo–O–Mo bridging bond.[42] Both XRD and FTIR results confirmed the high crystallinity of the samples.

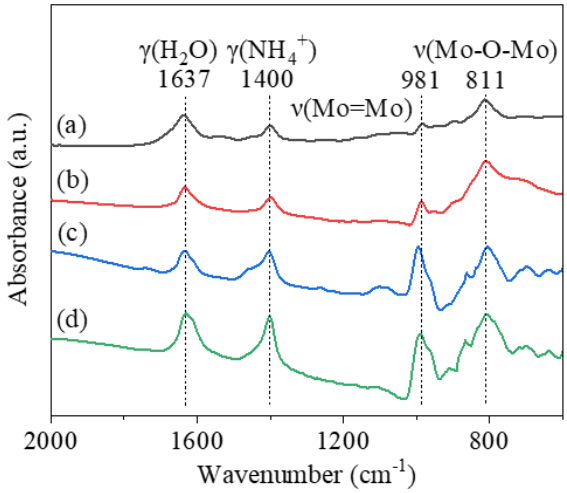


**Figure 2.** FTIR spectra of samples (a) MoVBiO-M-120, (b) MoVBiO-N-120, (c) MoVBiO-T-120 and (d) MoVBiO-T-175. All samples were heated at 80 °C for 12 h to remove the physically adsorbed water.

The porosity of the samples was examined by $N_2$ adsorption at 77 K (Figure 3). Samples MoVBiO-M-120, MoVBiO-N-120 and MoVBiO-T-120 show a combination of type I and IV isotherms containing a H1-type hysteresis.[43,44] The appearance of hysteresis loop is attributed to the voids formed by stacking of MoVBiO crystals.[45] Even though the samples were degassed at 300 °C for 2 h to open the channels, the pores of MoVBiO (seven-membered ring with a size of 0.34 nm), are too small for the $N_2$ to penetrate.[45] $N_2$ adsorption measurements were performed to evaluate the external surface area of the catalysts. The external surface area of samples

MoVBiO-M-120, MoVBiO-N-120, MoVBiO-T-120 and MoVBiO-T-175 is 36, 18, 12 and 8 $m^2 g^{-1}$, respectively (Table 1). The crystallinity of the samples is fully preserved before and after $N_2$ adsorption measurement (Figure S1), suggesting that the degassing process at 300 °C does not destroy the structure of samples.

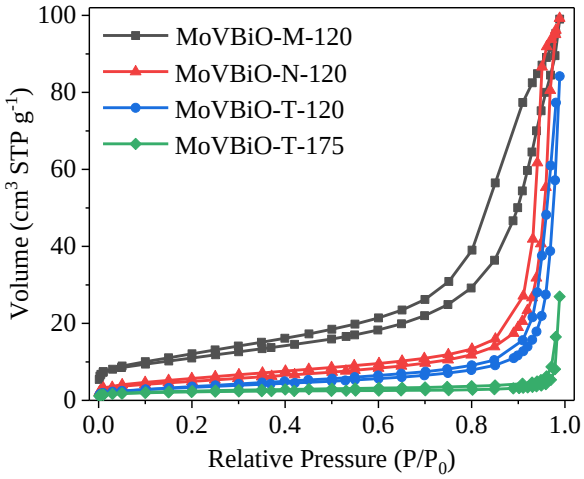


**Figure 3.** $N_2$ adsorption-desorption isotherms of samples MoVBiO-M-120, MoVBiO-N-120, MoVBiO-T-120 and MoVBiO-T-175.

The morphologies of the samples are presented in Figure 4. Samples MoVBiO-M-120, MoVBiO-N-120, MoVBiO-T-120 and MoVBiO-T-175 consist of aggregated crystals with an average size of about 35, 85, 115 and 310 nm, respectively. Additionally, the sizes of the crystals were calculated using the Scherrer equation based on the XRD results; the crystal sizes of the samples are consistent with the SEM observation (Table 1). The MoVBiO-M-120 was synthesized with methanol, while samples MoVBiO-T-120 and MoVBiO-T-175 were prepared with tartaric acid. The use of methanol resulted in a decrease of the crystal size, while the tartaric acid caused an increase of crystal size. The effects of the organic additives would be

further discussed in posterior section.

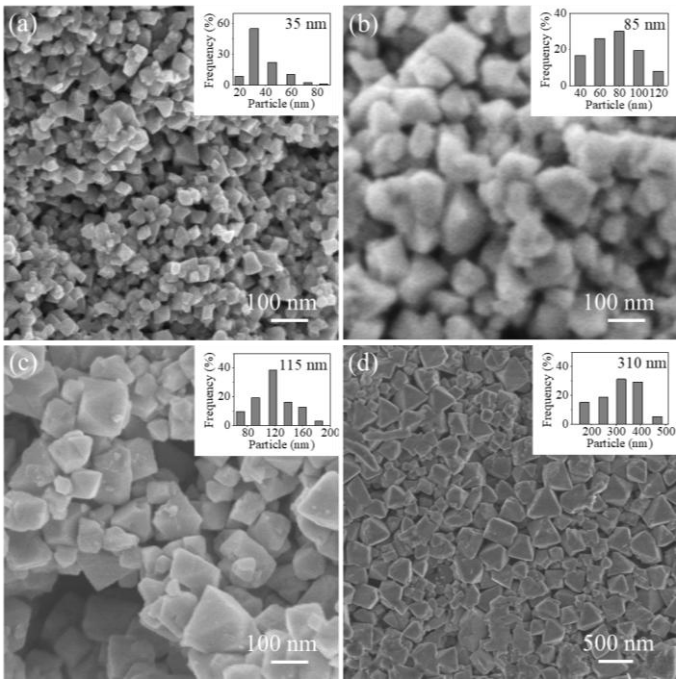


**Figure 4.** SEM images of samples (a) MoVBiO-M-120, (b) MoVBiO-N-120, (c) MoVBiO-T-120 and (d) MoVBiO-T-175. *Inset* of (a), (b), (c) and (d): particle size distribution determined by measuring of 200 particles.

**Table 1** Crystal size and specific surface area of samples MoVBiO-M-120, MoVBiO-N-120, MoVBiO-T-120 and MoVBiO-T-175.

| Sample | Size, XRD (nm)[a] | Size, SEM (nm)[b] | Size, TEM (nm)[c] | $S_{BET}$ ($m^2\ g^{-1}$)[d] |
|---|---|---|---|---|
| MoVBiO-M-120 | 30 | 35 | 33 | 36 |
| MoVBiO-N-120 | 65 | 85 | 70 | 18 |
| MoVBiO-T-120 | 77 | 115 | 100 | 12 |
| MoVBiO-T-175 | 102 | 310 | 300 | 8 |

[a] Size calculated using the Scherrer equation based on the full width at half maximum

of 2 Theta peak at 26.5°.

[b] Average size of particles measured by SEM.

[c] Average size of particles determined by TEM.

[d] Specific surface area measured by BET method.

TEM images of samples MoVBiO-M-120, MoVBiO-N-120, MoVBiO-T-120 and MoVBiO-T-175 are depicted in Figure 5; the crystal size is gradually increased in the order presented above. This observation is consistent with the XRD and SEM results (Figures 1 and 4; Table 1). The lattice fringes are clearly seen in the crystals, and the distance between two lattice fringes is 1.14 nm, corresponding to the (111) plane. These results confirmed the high crystallinity of the samples. Further, the distribution of molybdenum, vanadium and bismuth in the sample MoVBiO-M-120 is studied by HAADF-STEM-EDS (Figure 6). The HAADF-STEM-EDS result clearly showed the homogeneous distributions of the three elements (Mo, V and Bi). According to the HAADF-STEM-EDS, the ratio of Mo: V: Bi is 1: 0.43: 0.08, while according to the ICP-OES is 1: 0.34: 0.17. These measured ratios were close to the reported value of 1: 0.38: 0.21.[45]

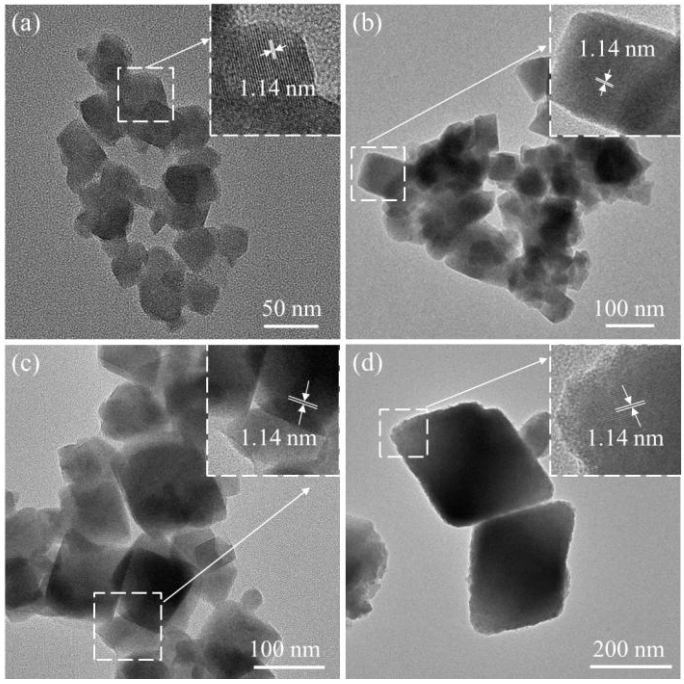


**Figure 5.** TEM images of samples (a) MoVBiO-M-120, (b) MoVBiO-N-120, (c) MoVBiO-T-120 and (d) MoVBiO-T-175. *Inset* of (a), (b), (c) and (d): enlarged area of the crystals.

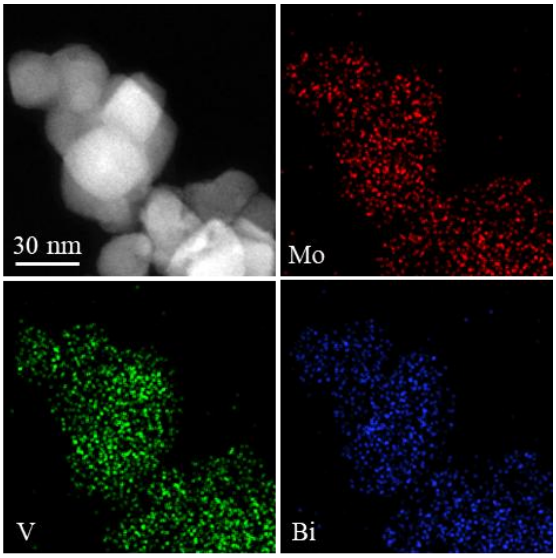


**Figure 6.** HAADF-STEM image and the corresponding HAADF-STEM-EDS elemental mapping of sample MoVBiO-M-120: Mo (red), V (green) and Bi (blue).

All the above results confirmed the successful synthesis of MoVBiO samples via

the assistance of organic additives with crystal sizes of 30–300 nm. The use of methanol increases while the tartaric acid decreases the crystal size of the samples.

In order to study the effect of methanol, the synthesis of a reference sample MoVBiO-N free of organic additive was performed. Figure 7 shows the TEM images of the precursor mixture containing only Mo, V and Bi prior to the crystallization. The sample prior to crystallization (MoVBiO-N) without methanol contains particles with a size of about 100 nm (Figure 7a). However, a large number of particles with an average size of 30 nm are observed in the sample containing methanol prior to the crystallization (Figure 7b). The average size of the amorphous particle is similar to the size of the crystalline material MoVBiO-M-120, i.e. 33 nm (Figure 7b and Table 1). The methanol accelerates the formation of particles due to the fast dissolution of Mo, V and Bi in the precursor leading to the formation of abundant, small-size crystals. Similar effects of methanol were reported for the synthesis of $Al(OH)_3$, $WO_3$ and ZSM-5.[46–48] Moreover, with increasing the crystallization time from 0 h to 48 h, the size of the crystals was preserved in the range of 30–40 nm (Figures 7b and 4a). This indicates that the crystallization time has a negligible effect on the crystal size of the samples in the presence of methanol.

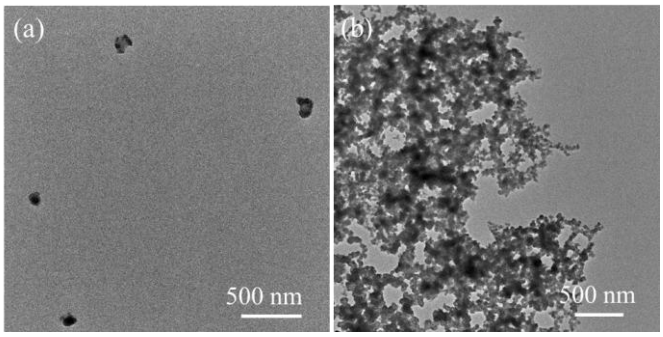


**Figure 7.** TEM images of particles extracted from the precursor mixtures used for the synthesis of samples (a) MoVBiO-N and (b) MoVBiO-M.

In the case of tartaric acid additive, the effect of crystallization time (4–48 h) at a constant synthesis temperature of 175 °C was studied; the SEM pictures of samples obtained at different crystallization times are shown in Figure S2. Sample MoVBiO-T-175 obtained after 4 h contains a mixture of both 200–400 nm octahedral particles and amorphous phase (Figure S2a). With increasing the crystallization time from 4 h to 12 h, the amorphous phase is gradually transformed to octahedral particles (Figure S2a–c). The morphology of the MoVBiO-T-175 crystals obtained after 24 h is similar to that obtained after 48 h, consisting of abundant 200–400 nm octahedral particles. The disappearance of amorphous phase and the formation of octahedral particles suggests the dissolution-crystallization mechanism.[49] As known, the complexation between tartaric acid and $Bi^{3+}$ is a useful strategy for designing of nanostructured Bi-based materials.[50,51] As previously stated, the Bi precursor was dissolved in the tartaric acid solution and thus the $Bi_2(C_4H_3O_6)_2$ organic complex was formed. The strong complexation between tartaric acid and $Bi^{3+}$ inhibited the nucleation of the crystals.[52,53] The limited crystal nuclei were beneficial to the

formation of large particles. Thus, we could conclude that the tartaric acid inhibited the nucleation and it is responsible for the formation of large MoVBiO-T-175 crystals.

In addition, samples MoVBiO-M-120 and MoVBiO-T-120 obtained at lower temperature were characterized by TG-MS analysis; the results are depicted in Figure 8. The weight loss of about 5% in two stages was measured. The first stage is in the range of 30–200 °C corresponding to the removal of physically adsorbed water.[54,55] In the second stage (200–370 °C), the peak at 354 °C (364 °C) is assigned to the water strongly bound to the framework.[55] No oxidation peaks of $CO_2$ formation are detected, which suggests that both methanol and tartaric acid additives are not present in the crystalline samples.

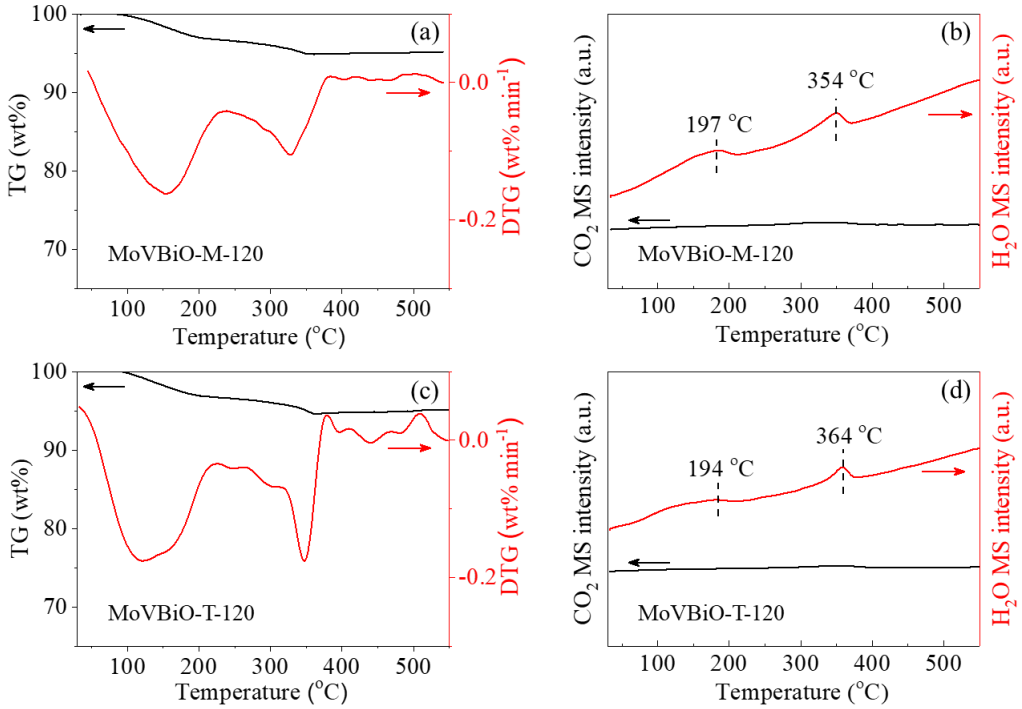


**Figure 8.** (a) TG/DTG and (b) MS curves of sample MoVBiO-M-120, and (c) TG/DTG and (d) MS of MoVBiO-T-120.

**MoVBiO catalysts for gas-phase indirect oxidation of methanol to methyl formate**

The evaluation of catalytic performance of the samples in indirect oxidation of methanol to MF was performed in a fixed-bed microreactor. As-synthesized samples (MoVBiO-M-120, MoVBiO-N-120, MoVBiO-T-120 and MoVBiO-T-175) were directly used in the catalytic tests without further modification. The $CH_3ONO$ conversion and MF selectivity as a function of the reaction temperature for the MF synthesis using a feed of $CH_3ONO/N_2$ (1/4, volume) at a GHSV of 6000 mL $g_{cat.}^{-1}$ $h^{-1}$ is depicted in Figure 9. The $CH_3ONO$ conversion increased gradually with increasing of the reaction temperature. When the temperature rose from 100 °C to 120 °C, the $CH_3ONO$ conversion on the MoVBiO-M-120 increased from 66.3% to 94.7%, and further increased to 99.1% at 160 °C. Both samples MoVBiO-M-120 and MoVBiO-N-120 show higher $CH_3ONO$ conversion than samples MoVBiO-T-120 and MoVBiO-T-175 possibly related to the crystal size and surface area of the samples (Table 1). The MoVBiO-T-175 exhibits the lowest MF selectivity while the MoVBiO-M-120 and MoVBiO-N-120 show higher MF selectivity in the temperature range of 100–160 °C. This is possibly associated with the acidity of the samples.[56,57] The main byproducts detected during all the catalytic tests are the dimethoxymethane and carbon monoxide.

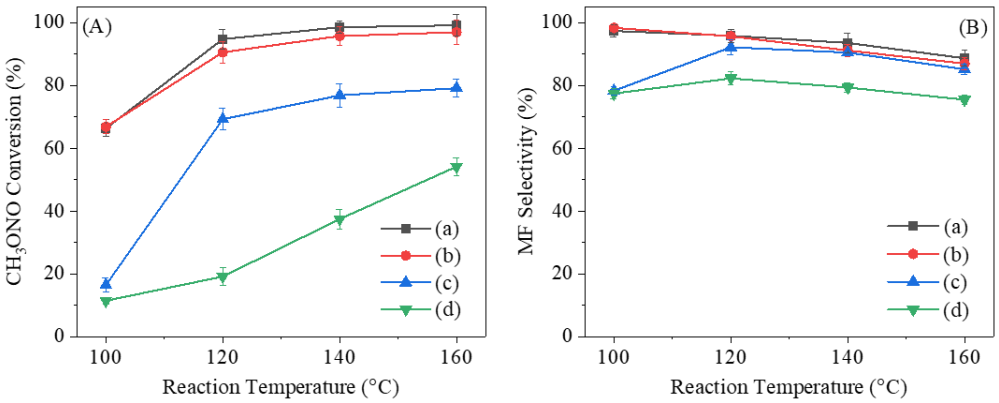


**Figure 9.** (A) $CH_3ONO$ conversion and (B) MF selectivity as a function of reaction temperature in the gas-phase indirect oxidation of methanol to MF using samples (a) MoVBiO-M-120, (b) MoVBiO-N-120, (c) MoVBiO-T-120 and (d) MoVBiO-T-175. Reaction conditions: 0.100 g catalyst; feed gas, $CH_3ONO/N_2$ = 1/4 (volume); GHSV = 6000 mL $g_{cat.}^{-1}$ $h^{-1}$; feed pressure = 0.1 MPa.

The DRIFTS spectra of pyridine absorbed on samples MoVBiO-M-120, MoVBiO-N-120, MoVBiO-T-120 and MoVBiO-T-175 are presented in Figure 10. The weak band at 1446 $cm^{-1}$ is assigned to the Lewis-bound pyridine.[58] The band at 1537 $cm^{-1}$ corresponds to Brønsted-bound pyridine, and the band at 1487 $cm^{-1}$ is assigned to pyridine associated with both Lewis and Brønsted acid sites.[58] Using the band areas of the peaks at 1446 $cm^{-1}$ and 1537 $cm^{-1}$, the Lewis and Brønsted acid sites are estimated, respectively (Table S1). Samples MoVBiO-M-120, MoVBiO-N-120, MoVBiO-T-120 and MoVBiO-T-175 contain similar amount of Lewis acid sites, but different Brønsted acid sites (Table S1). Therefore, the MF selectivity of the samples should be related with the different Brønsted acid sites. The MoVBiO-T-175 exhibits the highest amount of Brønsted acid sites while showed the

lowest MF selectivity (Figures 9 and 10). This is consistent with the previous result showing that the Brønsted acid sites led to the formation of the dimethoxymethane byproduct.[57] Moreover, sample MoVBiO-T-120 with the high amount of Brønsted acid sites shows lower MF selectivity than for samples MoVBiO-M-120 and MoVBiO-N-120 (Figures 9 and 10, Table S1).

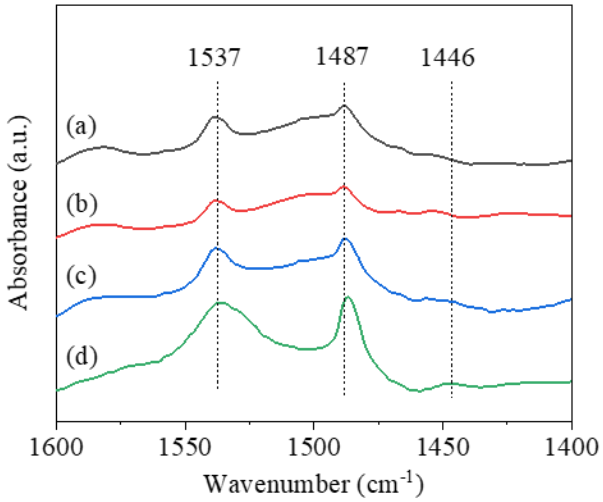


**Figure 10.** DRIFTS spectra of pyridine adsorbed on samples (a) MoVBiO-M-120, (b) MoVBiO-N-120, (c) MoVBiO-T-120 and (d) MoVBiO-T-175.

The apparent activation energies for the indirect oxidation of methanol to MF were measured in the temperature range of 115–135 ºC with an interval of 5 ºC. As presented in Table 2, the four catalysts (MoVBiO-M-120, MoVBiO-N-120, MoVBiO-T-120 and MoVBiO-T-175) show comparable activation energies of 38–50 kJ $mol^{-1}$ under the same reaction conditions. This indicates that the dominant reaction pathway and the rate-determining step are identical for all four catalysts.[58,59] Furthermore, samples MoVBiO-M-120 and MoVBiO-N-120 exhibit a high reaction rate of 48–50 mol $kg^{-1}$ $h^{-1}$, while samples MoVBiO-T-120 and MoVBiO-T-175 have

a low reaction rate of 35 and 8 mol $kg^{-1}$ $h^{-1}$, respectively (Table 2). As shown above, the crystal size of samples MoVBiO-M-120, MoVBiO-N-120, MoVBiO-T-120 and MoVBiO-T-175 is 33, 70, 100 and 300 nm as determined by TEM (Table 1). Clearly, the decreased reaction rate is in agreement with the increased crystal size of the samples (Tables 1 and 2). As known, the pores of MoVBiO (seven-membered ring with a size of 0.34 nm) are too small for the $CH_3ONO$ reactant to enter into the channels.[29] Thus the high $CH_3ONO$ conversion is contributed to the enhanced surface area of the samples providing more accessible surface active sites.

**Table 2** Catalytic performance of samples MoVBiO-M-120, MoVBiO-N-120, MoVBiO-T-120 and MoVBiO-T-175 in the indirect oxidation of methanol to MF.

| Sample | $CH_3ONO$ conversion (%)[a] | MF selectivity (%)[a] | $E_a$ (kJ $mol^{-1}$)[b] | $-r_{obs}$ (mol $kg^{-1}$ $h^{-1}$)[c] |
|---|---|---|---|---|
| MoVBiO-M-120 | 98.5 | 93.5 | 46 | 50 |
| MoVBiO-N-120 | 95.7 | 91.1 | 48 | 48 |
| MoVBiO-T-120 | 76.8 | 90.4 | 50 | 35 |
| MoVBiO-T-175 | 37.4 | 79.3 | 38 | 8 |

[a] The catalytic performance at 140 ºC shown in Figure 9.

[b] Apparent activation energy ($E_a$) calculated from the Arrhenius plots presented in Figure S3 (SI).

[c] Observed reaction rate ($-r_{obs}$).

The stability of the catalysts is of great importance in heterogeneous catalysts. A long-term catalytic test over the MoVBiO-M-120 sample was performed and the results are shown in Figure 11. The catalyst showed a high MF selectivity of about 94 ± 1% throughout 50 h test. However, the $CH_3ONO$ conversion is gradually decreased from 99% to 84% along the reaction time from 1 h to 50 h. The MoVBiO-M-120 after 50 h catalytic test was activated in air at 250 ºC for 3 h, and that catalyst showed an initial $CH_3ONO$ conversion of 98% (Figure S4). The $CH_3ONO$ conversion is gradually decreased from 98% to 88% with increasing the reaction time from 1 h to 12 h (Figure S4). The relatively slow but almost constant deactivation was assigned to the deposit of reaction species as described earlier.[58] The SEM images show that the crystals were preserved after 50 h test and the XRD patterns indicate a slight decrease in the crystallinity to 93% (Figures 11 and S5). Moreover, in comparison with the HY, γ-$Al_2O_3$, and $SiO_2$ catalysts reported in the literature,[30] the MoVBiO-M-120 exhibits the better catalytic performance (Table S2).

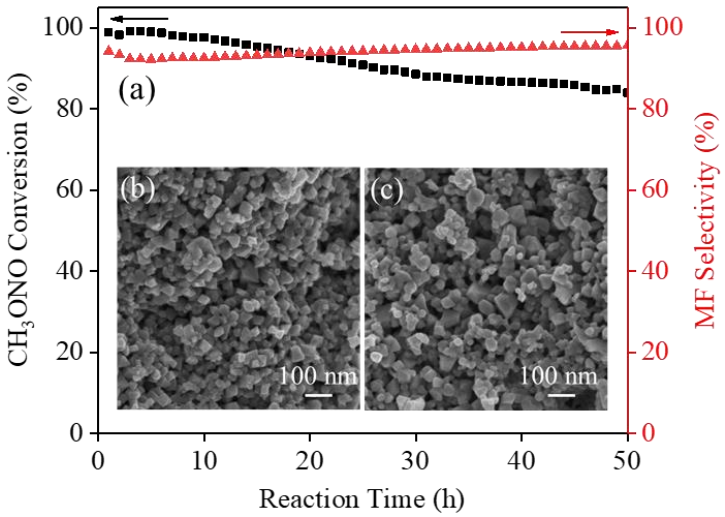


**Figure 11.** (a) $CH_3ONO$ conversion and MF selectivity measured for 50 h using the

MoVBiO-M-120 catalyst; SEM images of the MoVBiO-M-120 catalyst (b) before and (c) after 50 h catalytic test. Reaction conditions: 0.100 g catalyst; feed gas, $CH_3ONO/N_2$ = 1/4 (volume); GHSV = 6000 mL $g_{cat.}^{-1}$ $h^{-1}$; reaction temperature, 140 $^oC$; feed pressure = 0.1 MPa.

## Conclusion

MoVBiO samples with a size of 30–300 nm were synthesized in the presence of organic additives (methanol and tartaric acid). The use of methanol in the synthesis decreased the crystal size to 30 nm via facilitating the formation of small amorphous particles during the nucleation, while the tartaric acid increased the particle size to about 300 nm due to the complexation effect. The as-synthesized samples with different particle sizes were used in the indirect oxidation of methanol to methyl formate reaction. The high methyl nitrite conversion of about 92% and methyl formate selectivity of 94% are obtained at 140 °C for a feed gas of $CH_3ONO/N_2$ (1/4, volume) and with a gas hourly space velocity of 6000 mL $g_{cat.}^{-1}$ $h^{-1}$. The catalyst exhibited a relatively slow but almost constant deactivation over 50 h due to the deposit of reaction species. The Brønsted acid sites are found to be harmful for the methyl formate selectivity. The sample MoVBiO-M-120 with the smallest crystal size exhibits the highest conversion due to the large surface area and abundant accessible surface active sites.

## Experimental Section

### Catalyst preparation

Ammonium molybdate tetrahydrate ($(NH_4)_6Mo_7O_{24}\cdot 4H_2O$, 99.0 wt%), bismuth hydroxide ($Bi(OH)_3$, 90.0 wt%), bismuth nitrate ($Bi(NO_3)_3\cdot 5H_2O$, 99.0 wt%), methanol ($CH_3OH$) and tartaric acid ($HOOC(CHOH)_2COOH$, $C_4H_6O_6$) were purchased from Sinopharm Chemical Reagent Co., Ltd. Vanadyl sulfate ($VOSO_4\cdot 5H_2O$, 96.0 wt%) was purchased from Macklin Biochemical Co., Ltd.

The MoVBiO samples were synthesized using the procedure described earlier.[25] 2.73 g $(NH_4)_6Mo_7O_{24}\cdot 4H_2O$ (16.7 mmol based on Mo) was dissolved in 40 mL deionized water and 1.096 g $VOSO_4$ (4.2 mmol based on V) was dissolved in 40 mL deionized water and then the $VOSO_4$ solution was poured into the $(NH_4)_6Mo_7O_{24}\cdot 4H_2O$ solution. 0.161 g $Bi(OH)_3$ (0.56 mmol based on Bi) was added and then stirred for 10 min followed by $N_2$ bubbling to avoid oxidation. The pH of the mixture was adjusted to 3.7 with the addition of ammonia aqueous solution (28 wt%). The mixture was transferred into a 100 mL Teflon-lined autoclave and purged with $N_2$ for 10 min, and then subjected to heating at 120 °C for 48 h under static condition. The crystalline product was centrifuged (5000 r $min^{-1}$) and purified using a deionized water. The obtained solids were dried for 12 h at 80 °C. The final samples were denoted as MoVBiO-x-y, where “x” corresponds to the type of additive used in the synthesis process: x = N stands for no additive, x = M stands for methanol and x = T stands for tartaric acid; while y = 120 and 175 identifies the crystallization temperature of 120 °C and 175 °C, respectively. The as-obtained samples were

denoted as MoVBiO-N-120.

Adding methanol as an additive: 0.272 g $Bi(NO_3)_3 \cdot 5H_2O$ (0.56 mmol based on Bi) was dissolved in a 1.7 mL solution of methanol and water with a volume ratio of 1: 1. 2.73 g $(NH_4)_6Mo_7O_{24} \cdot 4H_2O$ (16.7 mmol based on Mo) was dissolved in 40 mL deionized water. 1.096 g $VOSO_4$ (4.2 mmol based on V) was dissolved in 40 mL deionized water. After stirring, the resulting $VOSO_4$ solution was poured into the solution of $(NH_4)_6Mo_7O_{24} \cdot 4H_2O$. Then, the $Bi(NO_3)_3$ precursor was added and stirred for 10 min followed by $N_2$ bubbling to avoid oxidation. The following steps were the same as the one used for the MoVBiO-N-120 sample. The obtained sample was denoted as MoVBi-M-120.

Adding tartaric acid as an additive: 0.292 g $C_4H_6O_6$ was dissolved in 5 mL deionized water. 0.161 g $Bi(OH)_3$ (0.56 mmol based on Bi) was dissolved in tartaric acid solution. 2.73 g $(NH_4)_6Mo_7O_{24} \cdot 4H_2O$ (16.7 mmol based on Mo) was dissolved in 35 mL deionized water. 1.096 g $VOSO_4$ (4.2 mmol based on V) was dissolved in 40 mL deionized water. After stirring, the resulting $VOSO_4$ solution was poured into solution of $(NH_4)_6Mo_7O_{24} \cdot 4H_2O$. Then, solution $Bi(OH)_3$ was added and stirred for 10 min followed by $N_2$ bubbling to avoid oxidation. The pH of the mixture was adjusted to 3.7 with 28 wt% of ammonia aqueous solution. The mixture was transferred into a 100 mL Teflon-lined autoclave and purged with $N_2$ for 10 min, and then subjected to heating at 120 °C and 175 °C for 48 h under static conditions. The following steps were the same as the one used for the MoVBiO-N-120. The obtained samples synthesized at 120 °C and 175 °C were denoted as MoVBi-T-120 and MoVBi-T-175,

respectively.

**Characterizations**

Powder X-ray diffraction (XRD) patterns were recorded on a Bruker D8 Advance diffractometer equipped with monochromated Cu Kα radiation (40 kV, 40 mA).

Fourier transform infrared (FTIR) spectra were recorded on a Bruker Vertex 70V spectrometer in the range of 400–4000 $cm^{-1}$ with 64 scans and a resolution of 4 $cm^{-1}$. Diffuse reflectance infrared Fourier transform spectroscopy (DRIFTS) spectra using pyridine were collected on a Nicolet-6700 spectrometer. The samples were dried at 300 °C for 3 h, followed by pyridine absorption at 25 °C for 24 h. After reaching an equilibrium, the samples were evacuated at 150 °C for 3 h to remove physically adsorbed pyridine. The absorbance spectra were recorded from 4000 $cm^{-1}$ to 650 $cm^{-1}$ with 64 accumulating scans and 4 $cm^{-1}$ resolution.

$N_2$ adsorption isotherms were obtained at 77 K with a Quantachrome Autosorb-1 analyzer. The samples were degassed under vacuum at 300 °C for 2 h prior to measurements. The specific surface area of the samples was calculated using the multi-point Brunauer-Emmett-Teller (BET) method.

Scanning electron microscopy (SEM) images were acquired on a JEOL JSM-7900F instrument. Transmission electron microscopy (TEM) images were recorded using a Thermo Scientific Talos F200X S/TEM instrument. High-angle annular dark-field scanning transmission electron microscopy (HAADF-STEM) images and elemental mapping were performed on a Thermo Scientific Talos F200X S/TEM instrument equipped with an energy dispersive X-ray spectrometer (EDS).

Elemental composition of the samples was determined by inductively coupled plasma optical emission spectroscopy (ICP-OES) on an Agilent 720 ICP-OES.

Thermogravimetric-mass spectrometry (TG-MS) study was performed on a NETZSCH QMS 403D instrument connected with STA 449 F5 mass spectrometer. The samples were heated from 40 °C to 550 °C with a heating rate of 10 °C $min^{-1}$ in an air flow of 50 mL $min^{-1}$.

**Reactivity tests**

The schematic diagram of the setup used for the catalytic test was presented in Scheme S2. The indirect oxidation of methanol to MF was performed in a continuous-flow fixed-bed microreactor with a quartz tube (8 mm diameter and 36 mm length) under 0.1 MPa. Quartz wool was placed below the bed to hold the catalyst. The $CH_3ONO$ reactant was synthesized though an esterification reaction ($2NaNO_2 + 2CH_3OH + H_2SO_4 \rightarrow 2CH_3ONO\uparrow + Na_2SO_4 + 2H_2O$) in the laboratory. The $CH_3ONO$ gas was collected into a steel cylinder and then mixed with pure $N_2$ to obtain a gas mixture of $CH_3ONO/N_2$ (1/4, volume). The pure $N_2$ and $CH_3ONO/N_2$ (1/4, volume) were fed via two calibrated mass flow meters, respectively. The temperature in the reactor was well-controlled with an inserted K-thermocouple in the range of 100–160 ºC. The composition of the outlet products was analyzed by an online Agilent 7890B gas chromatography. CO and $N_2$ were measured by a thermal conductivity detector (TCD) furnished with 2.5-m molecular sieve 5A and 1.0-m HayeSep Q packed columns. $CH_3ONO$, methanol, dimethoxymethane and MF were detected by a flame ionization detector (FID) with a 30-m HP-Innowax capillary

column. The calculations of the $CH_3ONO$ conversion, methyl formate (MF) selectivity, dimethoxymethane (DMM) selectivity, CO selectivity and reaction rate were presented in SI.

## Declaration of Competing Interest

The authors declare that they have no known competing financial interests or personal relationships that could have appeared to influence the work reported in this paper.

## Acknowledgements

This work was supported by the National Natural Science Foundation of China (21908246, 21975285, 22175200) and the International Research Network (IRN) “Zeolites”.

**References**


[1] L. Cronin, A. Müller, *Chem. Soc. Rev.* **2012**, *41*, 7325–7648.

[2] M. T. Pope, *Heteropoly and Isopoly Oxometalates*, Springer-Verlag, Berlin, **1983**.

[3] S. Roy, D. C. Crans, T. N. Parac-Vogt, *Front. Chem.* **2019**, *7*, 646.

[4] A. Dolbecq, P. Mialane, F. Secheresse, B. Keita, L. Nadjo, *Chem. Commun.* **2012**, *48*, 8299–8316.

[5] J. Song, Z. Luo, D. K. Britt, H. Furukawa, O. M. Yaghi, K. I. Hardcastle, C. L. Hill, *J. Am. Chem. Soc.* **2011**, *133*, 16839–16846.

[6] B. Nohra, H. El Moll, L. M. Rodriguez Albelo, P. Mialane, J. Marrot, C. Mellot-Draznieks, M. O'Keeffe, R. Ngo Biboum, J. Lemaire, B. Keita, *J. Am. Chem. Soc.* **2011**, *133*, 13363–13374.

[7] S. Uchida, E. Takahashi, N. Mizuno, *Inorg. Chem.* **2013**, *52*, 9320–9326.

[8] R. Eguchi, S. Uchida, N. Mizuno, *Angew. Chem. Int. Ed.* **2012**, *51*, 1635–1639; *Angew. Chem.* **2012**, *124*, 1667–1671.

[9] M. Zeng, K. Chen, J. Tan, J. Zhang, Y. Wei, *Front. Chem.* **2018**, *6*, 457.

[10] K. Suzuki, Y. Kikukawa, S. Uchida, H. Tokoro, K. Imoto, S. i. Ohkoshi, N. Mizuno, *Angew. Chem. Int. Ed.* **2012**, *51*, 1597–1601; *Angew. Chem.* **2012**, *124*, 1629–1633.

[11] Z. Zhang, Q. Zhu, M. Sadakane, T. Murayama, N. Hiyoshi, A. Yamamoto, S. Hata, H. Yoshida, S. Ishikawa, M. Hara, W. Ueda, *Nat. Commun.* **2018**, *9*, 3789.

[12] M. Sadakane, K. Kodato, T. Kuranishi, Y. Nodasaka, K. Sugawara, N. Sakaguchi, T. Nagai, Y. Matsui, W. Ueda, *Angew. Chem. Int. Ed.* **2008**, *47*, 2493–2496; *Angew. Chem.* **2008**, *120*, 2527–2530.

[13] C. Zhan, J. M. Cameron, D. Gabb, T. Boyd, R. S. Winter, L. Vilà-Nadal, S. G. Mitchell, S. Glatzel, J. Breternitz, D. H. Gregory, *Nat. Commun.* **2017**, *8*, 14185.

[14] Z. X. Zhang, S. Ishikawa, Y. Tsuboi, M. Sadakane, T. Murayama, W. Ueda, *Faraday Discuss.* **2016**, *188*, 81–98.

[15] Z. X. Zhang, M. Sadakane, T. Murayama, N. Sakaguchi, W. Ueda, *Inorg. Chem.* **2014**, *53*, 7309–7318.

[16] Z. Zhang, H. Wang, H. Yoshikawa, D. Matsumura, S. Hatao, S. Ishikawa, W. Ueda, *ACS Appl. Mater. Interfaces* **2020**, *12*, 6056–6063.

[17] S. Ishikawa, Y. Yamada, C. T. Qiu, Y. Kawahara, N. Hiyoshi, A. Yoshida, W. Ueda, *Chem. Mater.* **2019**, *31*, 1408–1417.

[18] T. Katou, D. Vitry, W. Ueda, *Catal. Today* **2004**, *91*, 237–240.

[19] S. Ishikawa, T. Murayama, M. Kumaki, M. Tashiro, Z. X. Zhang, A. Yoshida, W. Ueda, *Top. Catal.* **2016**, *59*, 1477–1488.

[20] Z. Zhang, M. Sadakane, S.-i. Noro, T. Murayama, T. Kamachi, K. Yoshizawa, W. Ueda, *J. Mater. Chem. A* **2015**, *3*, 746–755.

[21] X. Liu, W. Gong, J. Luo, C. Zou, Y. Yang, S. Yang, *Appl. Surf. Sci.* **2016**, 517–524.

[22] C. Dey, R. Das, P. Pachfule, P. Po Dd Ar, R. Banerjee, *Cryst. Growth Des.*

**2011**, *11*, 139–146.

[23] W. Ueda, Y. Endo, N. Watanabe, *Top. Catal.* **2006**, *38*, 261–268.

[24] Z. Zhang, D. Li, Q. Zhu, M. Hara, Y. Li, W. Ueda, *New J. Chem.* **2021**, *45*, 21624–21630.

[25] Z. X. Zhang, M. Sadakane, T. Murayama, S. Izumi, N. Yasuda, N. Sakaguchi, W. Ueda, *Inorg. Chem.* **2014**, *53*, 903–911.

[26] J. M. Thomas, R. Raja, G. Sankar, R. G. Bell, *Nature* **1999**, *398*, 227–230.

[27] J. M. Thomas, R. Raja, *PNAS* **2005**, *102*, 13732–13736.

[28] S. Ishikawa, Y. Goto, Y. Kawahara, S. Inukai, N. Hiyosh, N. F. Dummer, T. Murayama, A. Yoshida, M. Sadakane, W. Ueda, *Chem. Mater.* **2017**, *29*, 2939–2950.

[29] S. Ishikawa, Z. Zhang, W. Ueda, *ACS Catal.* **2018**, *8*, 2935–2943.

[30] G. L. Zhuo, X. Z. Jiang, *Catal. Lett.* **2002**, *80*, 171–174.

[31] D. Kaiser, L. Beckmann, J. Walter, M. Bertau, *Catalysts* **2021**, *11*, 869.

[32] E. Tronconi, A. S. Elmi, N. Ferlazzo, P. Forzatti, G. Busca, P. Tittarelli, *Ind. Eng. Chem. Res.* **1987**, *26*, 1269–1275.

[33] L. Rong, Z. Xu, J. Sun, G. Guo, *J. Energy Chem.* **2018**, *27*, 238–242.

[34] K.-D. Jung, O.-S. Joo, S.-H. Han, S.-J. Uhm, I.-J. Chung, *Catal. Lett.* **1995**, *35*, 303–311.

[35] N. Wang, Y. Quan, J. Zhao, H. Li, J. Ren, *Mol. Catal.* **2021**, *505*, 111514.

[36] Q. Zhang, C. Zhu, G. Yang, Y. Sun, D. Wang, J. Liu, *Catal. Commun.* **2019**, *129*, 105741.

[37] N. Westhues, M. Belleflamme, J. Klankermayer, *ChemCatChem* **2019**, *11*, 5269–5274.

[38] J. J. Corral-Pérez, A. Bansode, C. S. Praveen, A. Kokalj, H. Reymond, A. Comas-Vives, J. VandeVondele, C. Copéret, P. R. von Rohr, A. Urakawa, *J. Am. Chem. Soc.* **2018**, *140*, 13884–13891.

[39] C. Li, X. Yang, G. Gao, Y. Li, W. Zhang, X. Chen, H. Su, S. Wang, Z. Wang, *Catal. Sci. Technol.* **2019**, *9*, 6240–6252.

[40] Q. Guo, C. Xu, W. Yang, Z. Ren, Z. Ma, D. Dai, T. K. Minton, X. Yang, *J. Phys. Chem. C* **2013**, *117*, 5293–5300.

[41] Y. Yamamoto, *Catal. Surv. Asia* **2010**, *14*, 103–110.

[42] Z. X. Zhang, S. Ishikawa, Q. Q. Zhu, T. Murayama, M. Sadakane, M. Hara, W. Ueda, *Inorg. Chem.* **2019**, *58*, 6283–6293.

[43] L. Zhao, G. Yang, H. Guo, C. Wang, L. Wang, S. Mintova, *Chem. Res. Chin. Univ.* **2021**, *37*, 1137–1142.

[44] H. Awala, J.-P. Gilson, R. Retoux, P. Boullay, J.-M. Goupil, V. Valtchev, S. Mintova, *Nat. Mater.* **2015**, *14*, 447–451.

[45] Z. X. Zhang, M. Sadakane, T. Murayama, W. Ueda, *Dalton Trans.* **2014**, *43*, 13584–13590.

[46] Z. G. Zhao, Z. F. Liu, M. Miyauchi, *Chem. Commun.* **2010**, *46*, 3321–3323.

[47] Y. Zhang, S. Zheng, H. Du, H. Xu, S. Wang, Y. Zhang, *Hydrometallurgy* **2009**, *98*, 38–44.

[48] X. Zhou, X. Cui, H. Chen, Y. Zhu, Y. Song, J. Shi, *Dalton Trans.* **2012**, *42*,

890–893.

[49] G. Oskam, *J. Sol-Gel Sci. Technol.* **2006**, *37*, 161–164.

[50] P. Morandi, V. Flaud, S. Tingry, D. Cornu, Y. Holade, *J. Mater. Chem. A* **2020**, *8*, 18840–18855.

[51] C. W. Lee, J. S. Hong, K. D. Yang, K. Jin, J. H. Lee, H.-Y. Ahn, H. Seo, N.-E. Sung, K. T. Nam, *ACS Catal.* **2018**, *8*, 931–937.

[52] A. A. Bode, P. G. Pulles, M. Lutz, W. J. Poulisse, S. Jiang, J. A. Meijer, W. J. van Enckevort, E. Vlieg, *Cryst. Growth Des.* **2015**, *15*, 3166–3174.

[53] L. Tan, A. Tang, X. Wen, J. Wang, Y. Liu, *CrystEngComm* **2017**, *19*, 2852–2859.

[54] M. Sadakane, S. Ohmura, K. Kodato, T. Fujisawa, K. Kato, K.-i. Shimidzu, T. Murayama, W. Ueda, *Chem. Commun.* **2011**, *47*, 10812–10814.

[55] S. Ishikawa, D. Kobayashi, T. Konya, S. Ohmura, T. Murayama, N. Yasuda, M. Sadakane, W. Ueda, *J. Phys. Chem. C* **2015**, *119*, 7195–7206.

[56] S. Huang, B. Yan, S. Wang, X. Ma, *Chem. Soc. Rev.* **2015**, *44*, 3079–3116.

[57] Y. Dong, S. Huang, S. Wang, Y. Zhao, J. Gong, X. Ma, *ChemCatChem* **2013**, *5*, 2174–2177.

[58] C. Wang, W. Xu, Z. Qin, H. Guo, X. Liu, S. Mintova, *J. Energy Chem.* **2021**, *52*, 191–201.

[59] C. Wang, N. Xu, T.-T. Liu, W. Xu, H. Guo, Y. Li, P. Bai, X.-P. Wu, X.-Q. Gong, X. Liu, S. Mintova, *J. Catal.* **2021**, *396*, 269–280.

**Table of Contents**

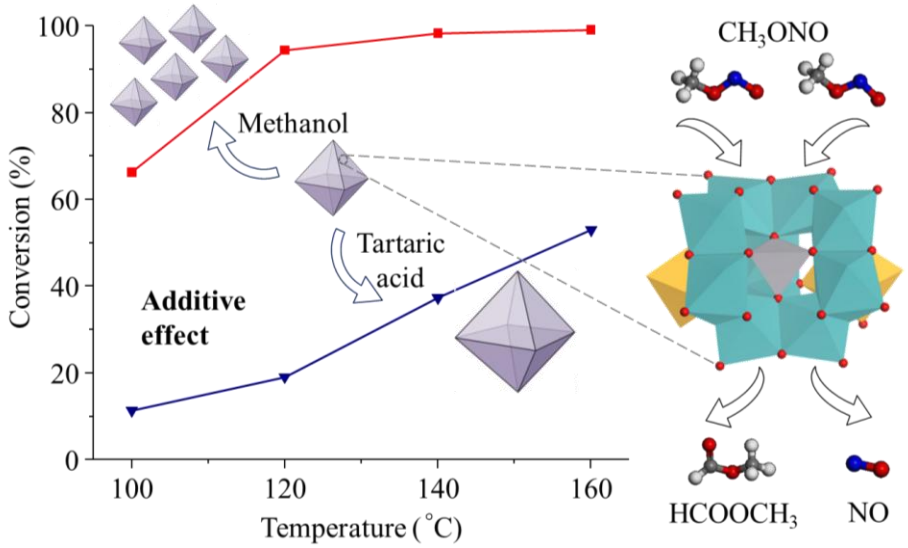


Crystalline porous MoVBiO was tuned in the range of 30-300 nm using organic additives. Methanol could decrease the crystal size to 30 nm while tartaric acid increased the size to 300 nm. The MoVBiO with small size showed higher methyl nitrite conversion and methyl formate selectivity than that with large size, as the result of more accessible surface active sites.